[redacted]

Copy
RM L9K01a

[redacted]L

NACA RM L9K01a

[redacted]

TECH LIBRARY KAFB, NM
0143806

NACA

RESEARCH MEMORANDUM

7183

ROCKET-POWERED FLIGHT TEST OF A ROLL-STABILIZED SUPERSONIC MISSILE CONFIGURATION

By Robert A. Gardiner and Jacob Zarovsky

Langley Aeronautical Laboratory
Langley Air Force Base, Va.

CLASSIFIED DOCUMENT

[redacted]

HOLLOMAN AFB N. M.

NATIONAL ADVISORY COMMITTEE FOR AERONAUTICS

WASHINGTON

January 12, 1950

[redacted]AL

[redacted]

Classification cancelled (or changed to Unclassified)

By authority of NASA Tech Pub Announcement 93 30 Oct 65

By .....

OFFICER AUTHORIZED TO CHANGE

NK

GRADE OF OFFICER MAKING CHANGE)

16 Apr 62

DATE

[redacted]

E R R A T U M

NACA RM L9K01a

ROCKET-POWERED FLIGHT TEST OF A ROLL-STABILIZED SUPERSONIC MISSILE CONFIGURATION

By Robert A. Gardiner and Jacob Zarovsky

January 12, 1950

Page 8, line 10: The value -0.034 should be changed to -0.025.

[redacted]

NACA-Langley - 2-16-50 - 400

[redacted]

RECEIVED
24 FEB 1950
HOLLOMAN
AFB N. M.

TECH LIBRARY KAFB, NM
0143806

 [redacted]

NATIONAL ADVISORY COMMITTEE FOR AERONAUTICS

RESEARCH MEMORANDUM

ROCKET-POWERED FLIGHT TEST OF A ROLL-STABILIZED SUPERSONIC MISSILE CONFIGURATION

By Robert A. Gardiner and Jacob Zarovsky

SUMMARY

The results of a flight at supersonic speed of an automatically roll-stabilized rocket-powered model incorporating a gyro-actuated control system in combination with wing-tip ailerons are reported. The autopilot consisted of a gyroscope directly coupled to the ailerons, the hinge-moment torque being supplied by an auxiliary torque motor which operated to precess the gyroscope to its centered position.

It is concluded that the combination of wing-tip ailerons and gyro-actuated control system is a satisfactory method of obtaining roll stabilization during zero-lift supersonic flight and that the method of calculating rolling response by using a single-degree-of-freedom equation is valid for zero-lift flight.

INTRODUCTION

The Pilotless Aircraft Research Division of the National Advisory Committee for Aeronautics has undertaken a series of automatic-stabilization tests. The object of the flight test reported herein was to test the gyro-actuated control system in combination with wing-tip ailerons at supersonic speeds. The autopilot consisted of a gyroscope directly coupled to the ailerons, the hinge-moment torque being supplied by an auxiliary torque motor which operated to precess the gyroscope to its centered position. The autopilot combines mechanical simplicity and essentially zero-lag operation over a range of operating conditions. This autopilot is of the same type as the one used to stabilize successfully a subsonic missile model as described in reference 1.

In order to test this roll-stabilization system in zero-lift supersonic flight, the measured autopilot characteristics were combined with

[redacted]

[redacted]

the estimated aerodynamic and mass characteristics of the missile model for preflight system analysis. System redesign was based on the analysis. The improved system was first bench tested, then tested in free flight. An auxiliary pair of ailerons was pulsed in a "square-wave" pattern to provide roll disturbances in flight so that the stabilization-system performance could be determined.

The rocket-powered model was launched at the Langley Pilotless Aircraft Research Station at Wallops Island, Va.

SYMBOLS

t time, seconds (zero time for flight records is from time of booster rocket firing)

X airframe axis coinciding with body center line

Y airframe axis which passes through center of gravity and lies in plane of horizontal wings

Z airframe axis which passes through center of gravity and is perpendicular to X- and Y-axes

I_X moment of inertia about the X-axis, slug-feet^2

I_Y moment of inertia about the Y-axis, slug-feet^2

I_Z moment of inertia about the Z-axis, slug-feet^2

S_w wing area in one plane bounded by extension of leading and trailing edges to center line of model, 4.1 square feet

S_b body frontal area, 0.35 square foot

$S_t = 2S_w$

c wing chord, 1.77 feet

b wing span, feet

V velocity, feet per second

q dynamic pressure, pounds per square foot $\left(\frac{1}{2}\rho V^2\right)$

ρ density, slugs/cubic foot

α angle of attack, positive when body axis is above relative wind vector, degrees

φ roll angle, positive in roll to right, degrees

p, $\dot{\varphi}$ roll angular velocity, positive to right, degrees per second $\left(\frac{d\varphi}{dt}\right)$

ϵ error signal $\left(\varphi_i - \varphi_o\right)$

δ_a total differential aileron angle, positive when trailing edge of right aileron is down, degrees

L rolling moment, positive to the right, subscripts $\dot{\varphi}$ and δ_a refer to variation of rolling moment with $\dot{\varphi}$ and δ_a, $\frac{\partial L}{\partial \dot{\varphi}}$ and $\frac{\partial L}{\partial \delta_a}$, respectively, foot pounds

$C_{l_{\delta_a}}$, variation of rolling-moment coefficient with aileron angle $\left(\frac{L_{\delta_a}}{qS_w b}\right)$

C_{l_p} variation of rolling-moment coefficient with rolling-angular-velocity factor $\left(\frac{L_{\dot{\varphi}}}{qS_t b\left(\frac{b}{2V}\right)}\right)$

K control gearing ratio - static value of $\frac{\delta_a}{\varphi}$

C_m pitching-moment coefficient $\left(\frac{\text{Pitching moment}}{qS_w c}\right)$

C_{m_α} variation of pitching-moment coefficient with angle of attack $\left(\frac{\partial C_m}{\partial \alpha}\right)$

ω frequency, radians per second

M Mach number

a_n normal acceleration, positive upward $\left(\frac{\text{Linear acceleration}}{g}\right)$

g acceleration due to gravity

δ_e elevator deflection, positive when trailing edge is down

Subscripts:

$\delta_a' = \frac{\delta_a}{2}$

o output

i input

L left aileron angle only

R right aileron angle only

METHODS AND APPARATUS

Model.- The airframe used in the analysis and flight test described herein was an all-metal missile research model. A sketch of the configuration and some physical properties are shown in figure 1. A photograph of the configuration is included as figure 2. The canard fins were fixed, and the wing-tip ailerons, figure 1(b), were movable. One pair of ailerons was used for control, being connected to the autopilot through a mechanical linkage. The other pair of ailerons was connected to a large solenoid through a spring return and differential linkage and was pulsed in a square-wave pattern to provide roll disturbances in flight.

The model was equipped with an NACA six-channel telemeter. Information telemetered included rate of roll, control-aileron position, total head, static pressure, normal acceleration, transverse acceleration, and indications of pulse-aileron operation and autopilot torque-motor operation which were obtained by displacing the reference value of the static-pressure and acceleration channels.

The booster used to bring the model up to supersonic speed was a 6000-pound-thrust, 3-second-duration, solid-propellant rocket. An adaptor fitting on the front end of the booster assembly provided a roll-free mounting for the model so that out-of-trim rolling moments of the booster would not affect the model during the boost phase.

Autopilot.- The autopilot was designed to act under all conditions to return the airframe to a trimmed-roll position, provided that the

rolling moment available from the control ailerons was not exceeded by out-of-trim and applied roll disturbances. The autopilot, shown in figure 3, consisted of a position gyroscope with two degrees of gimbal freedom (directly connected to the control ailerons through a slotted cam and rider) and an electric torque motor. The cam was arranged so that in the usable control range the lift of the cam caused the aileron deflection to be proportional to the roll angle and in such a direction as to return the airframe to a roll angle corresponding to the center of the usable control range. Through this control range the autopilot operation is described by the equation $\delta_a = -K\varphi$, where K is a proportionality factor and the minus sign denotes corrective control.

Outside of the usable control range, constant aileron deflection is maintained since the cam has zero slope. The cam return (180° away from the usable control range) causes the aileron deflection to be proportional to the roll angle; however, in this case the rolling moment produced by the ailerons causes the airframe to roll away from the cam return. Thus, at all angles of bank the aileron deflection is of such a sign as to produce a rolling moment which will restore the airframe to the center of the usable control range. The limits of control-aileron deflection (the zero-slope portion of the cam) were set at $\pm 10^\circ$ since it was estimated that this range would be sufficient to overcome the rolling moment due to probable construction asymmetry and to the pulsed ailerons. The proportionality factor K has a strong influence on the stability and transient performance of the roll-stabilized system. The adjustment of this factor is of primary importance. The value of K equal to 0.6, which would produce satisfactory performance, was found by the method shown in the appendix.

In the normal operating sequence, when the model was disturbed from its initial roll position, the autopilot caused the control ailerons to be deflected according to the description given previously. The presence of hinge moment on the ailerons and friction in the mechanical linkage then caused the inner gimbal of the gyroscope to precess, the direction and rate of precession depending upon the magnitude and direction of the torque applied to the outer gimbal by the control ailerons and linkage. Precession of the inner gimbal caused a contact to be made which closed a relay and energized the electric torque motor. The torque motor then applied a counteracting torque to the outer gimbal, causing the inner gimbal to precess toward its centered position.

An additional description of the operating principle of the autopilot appears in reference 1.

Preflight measurements.- The values found in model preflight measurements are shown below:

Model weight, lb 158.5

Moments of inertia:

I_X, slug-ft^2 . . . . . 0.8

I_Y, slug-ft^2 . . . . . 37.66

I_Z, slug-ft^2 . . . . . 37.16

Control gearing ratio, K 0.577

Control-aileron no-load maximum deflections:

δ_{a_L} . . . . . 4.2° to -5°

δ_{a_R} . . . . . 4.0° to -5°

Pulsed-aileron no-load deflections total angles:

δ_a . . . . . 4.25°

δ_a . . . . . -5°

Period of pulse ailerons, sec/cycle 0.77

Flight.- The model was launched at an angle of approximately 60° from the horizontal. Normal drag separation occurred at booster burnout, and the model coasted for the remainder of the flight. In addition to the telemeter, radar tracking was employed to obtain flight data. Photographs were taken of the launching and a high-speed motion-picture camera tracked the model during the flight.

RESULTS AND DISCUSSION

Roll stabilization.- Sections of the telemeter record obtained from the flight test are shown as figures 4 and 5. Figure 4 is included as a typical portion of record obtained in supersonic flight. It may be noted that the control-aileron deflection remained constant for a portion of a pulse half-cycle, indicating a roll angle greater than approximately $\frac{10^\circ}{K}$ (17.3°) for this portion. Figure 5 shows the roll velocity and control-aileron deflection records before, during, and after booster separation. The time of separation is not apparent on these records since the roll-free connection of the model to the booster had only a small effect on the model roll characteristics.

The fact that the ailerons and control gyroscope are directly coupled through the autopilot will allow the conversion of the measured

aileron angle to roll angle through the use of the control-gearing-ratio constant. This may be done and roll angle may be plotted from the telemeter record except at those values of aileron deflection great enough so that the cam follower is on the flat part of the cam. At these large values of aileron deflection the roll angle cannot be determined except by integrating the roll-velocity record. Attempts to determine the roll position by integration of roll velocity resulted in poor agreement with the roll position determined from the control-aileron angle. This was due to the errors involved in integration of the roll-velocity telemeter record. The accuracy of the roll-velocity record is estimated to be 10° per second. It can be noted that successful roll stabilization was secured since the rolling-velocity plot (fig. 4) tends to return to zero rolling rate near the end of the pulse half-cycle in the case where the flat of the cam was reached. The telemeter record showed that the model was roll-stabilized throughout the boost phase of the flight, at booster separation - where the maximum Mach number of 1.38 occurred, and in the speed region of interest, that is, to a Mach number of 0.8. This stabilization was obtained during essentially zero-lift flight.

It is possible to determine values of the damping-in-roll derivative C_{l_p} and the roll-control-effectiveness derivative $C_{l_{\delta_a}}$, for the configuration from portions of the record in which $\delta_a = -K\varphi$. This was done for each pulse half-cycle in which a sufficient number of peaks occurred in the rate-of-roll record to allow reasonable accuracy. The values of C_{l_p} and $C_{l_{\delta_a}}$, so derived are included as figure 6 and are compared with unpublished values found for a similar configuration. These values were obtained by using a different technique than the one used herein and for a configuration with the canard fins removed. The roll-control-effectiveness derivative is presented as $C_{l_{\delta_a}}$, plotted against Mach number in agreement with the conventional aerodynamic definition of the derivative. As a check, the derivatives determined were substituted in the single-degree-of-freedom roll equation and the system response to a pulsed-aileron disturbance calculated for a portion of the record. The V and q values used in the check calculation were determined from the flight record at an average Mach number for the pulse half-cycle. The calculated and experimental rate-of-roll plots are in good agreement, as shown in figure 7. The conclusion may be formed that the calculations are valid for zero-lift flight.

Hinge moments.- The precessional velocity of the control gyroscope in a gyro-actuated control is directly proportional to the hinge moment. Since this is so, it was thought that the frequency of torque-motor pulsing would be proportional to hinge moment. A ground calibration of the torque-motor-pulsing frequency against aileron hinge moment

confirmed this surmise. During the flight the actual hinge moments from the wing-tip ailerons were small so that no quantitative measure of hinge moment could be obtained. It was noted from the telemeter record, however, that the hinge moment is very low in the speed region of $M = 1.38$ and increases as the velocity decreases.

Longitudinal stability.- It was found that by using a single-degree-of-freedom equation a value of the static longitudinal derivative C_{m_α} could be determined from the longitudinal oscillation which appeared on the normal-accelerometer channel at booster separation (fig. 8). This value was found to be -0.034 per degree at an average $M = 1.34$. Since the primary purpose of this research missile configuration is automatic-stabilization work, the frequency response is of interest. By the use of the method presented in reference 2, the longitudinal oscillation was reduced to frequency-response form and is presented as such in figure 9.

Drag.- The drag of the canard model tested is presented in figure 10 as a plot of drag coefficient (C_D) against Mach number. For comparison purposes, the unpublished drag data for a conventional missile airframe are included on the figure. The conventional airframe and the roll-stabilized canard model have the same fineness ratio body, approximately the same nose shape, and are of comparable size. The only appreciable difference in the drag of the two configurations appears in the high-subsonic Mach number range, where the canard model exhibits an earlier, more gradual drag rise. Other unpublished data indicate that this early drag rise may be due to the thick tip section of the canard-model wing.

The conventional airframe has a constant 4-percent-thickness-ratio wing, whereas the canard-model wing thickness ratio varied from 3 percent at the root to 9 percent at the tip. The tip thickness was governed by the required strength of the torque rods which actuated the wing-tip ailerons and is inherent in the configuration.

It should be noted that the drag of the conventional airframe was determined from free-flight testing of a research model at zero lift and with zero control-surface deflection; the canard model was flown with an average of about 10° of aileron deflection.

CONCLUSIONS

As a result of the flight test it may be concluded that the use of the combination of a delta-wing configuration equipped with wing-tip ailerons and gyro-actuated control system is a satisfactory method of obtaining roll stabilization during zero-lift supersonic and transonic flight.

The method of calculating rolling response by using a single-degree-of-freedom equation for the autopilot and airframe is valid for zero-lift flight.

Langley Aeronautical Laboratory
National Advisory Committee for Aeronautics
Langley Air Force Base, Va.

APPENDIX

ANALYTICAL METHODS

The airframe and autopilot combination was analyzed according to servomechanism theory as a feedback system. The block diagram of the system is shown as follows:

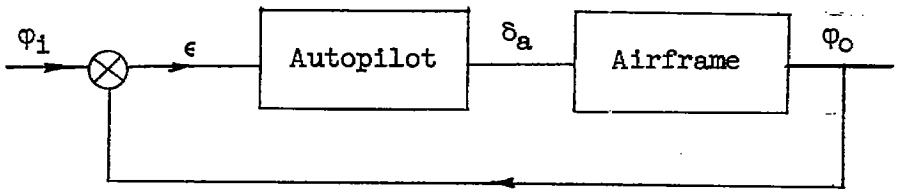

The airframe frequency response was calculated by making the substitution $D = i\omega$ in the single-degree-of-freedom roll equation $\varphi\left(I_X D^2 - L_{\dot{\varphi}} D\right) = \delta_a L_{\delta_a}$ where the differential operator $D = \frac{d}{dt}$. The values of the derivatives C_{l_p} and $C_{l_{\delta_a}}$, were the best possible estimates based on available wind-tunnel data for similar configurations. The moment of inertia about the X-axis was estimated from the design mass distribution. Estimated values of the parameters used in the airframe frequency-response calculations are shown in table I.

The frequency response of the autopilot was measured from oscillating table tests under several simulated hinge-moment loadings. The method used in measuring the autopilot frequency response is that described in reference 3. A photograph of the autopilot test setup is shown in figure 11.

Under no-load conditions, the autopilot frequency response was of unit amplitude and zero phase over the frequency range up to 20 cycles per second. Under the maximum hinge-moment test conditions, it was found that bending in the linkage caused a slight variation from the unit-amplitude, zero-phase response. Since the maximum simulated hinge moment was greater than that expected in flight and the frequency-response variation with hinge moment was small, the no-load response of the autopilot was used in the analysis.

The autopilot initial design fixed the control gearing ratio at 1.0. When the combined autopilot-airframe frequency response was plotted as a Nyquist diagram it was found that, although stable, the amount of phase

margin (reference 4) was insufficient, this fact indicating a very oscillatory system transient response. The control gearing ratio was then reduced to 0.6; the resulting Nyquist diagram, shown in figure 12, had a satisfactory phase margin and indicated an improved transient response. As a final check the system transient response to a step input of aileron deflection was calculated by the method of reference 2, which, in this case, produced the somewhat erratic transient curve shown in figure 13.

REFERENCES

1. Teitelbaum, Jerome M., and Seaberg, Ernest C.: An Experimental Investigation of a Gyro-Actuated Roll Control System Installed in a Subsonic Test Vehicle. NACA RM L9B24a, 1949.

2. Seamans, Robert C., Jr., Bromberg, Benjamin G., and Payne, L. E.: Application of the Performance Operator to Aircraft Automatic Control. Jour. Aero. Sci., vol. 15, no. 9, Sept. 1948, pp. 535-555.

3. Seaberg, Ernest C.: Laboratory Investigation of an Autopilot Utilizing a Mechanical Linkage with a Dead Spot to Obtain an Effective Rate Signal. NACA RM L9F15a, 1949.

4. Brown, Gordon S., and Campbell, Donald P.: Principles of Servomechanisms. John Wiley & Sons, Inc., 1948, p. 189.

TABLE I

ESTIMATED AIRFRAME PARAMETERS USED IN

PREFLIGHT SYSTEM ANALYSIS

I_X, slug-ft^2	0.54
L_{δ_a}, ft-lb/radian	-1262
$L_{\dot{\phi}}$, ft-lb/radian/sec	-12.22
b, ft	3.08
V, ft/sec	1963
q, lb/ft^2	4270
M	1.8

Note: δ_a is the total differential angle of the control ailerons.

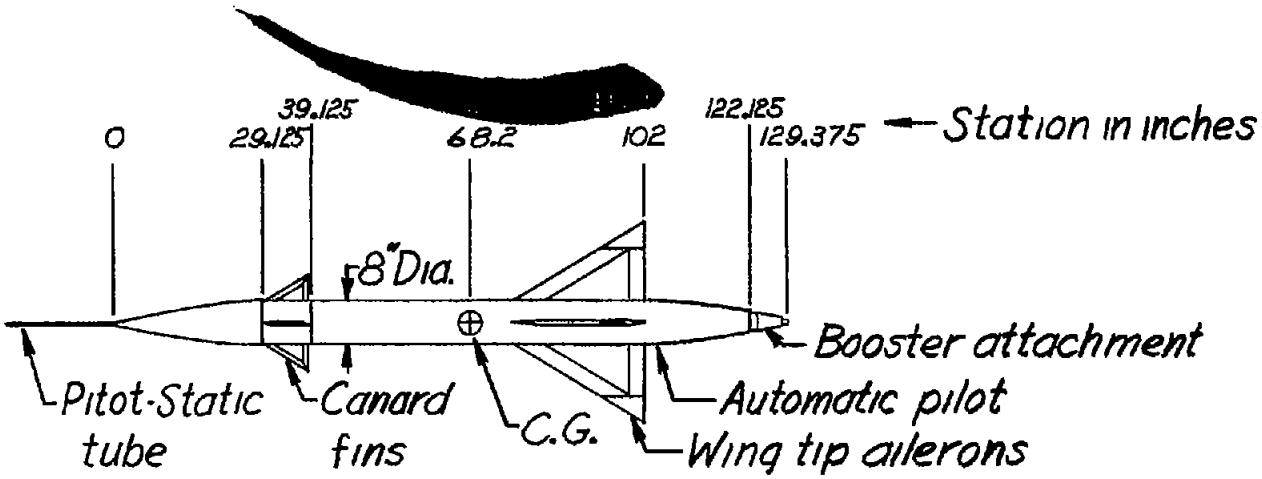

Airframe

Wing span, b, in.	37
Canard fin span, in.	17.667
Wing area per plane, S_w, ft^2	4.1
Total included wing area, S_t, ft^2 . . .	8.2
Body frontal area, S_f, ft^2	0.35

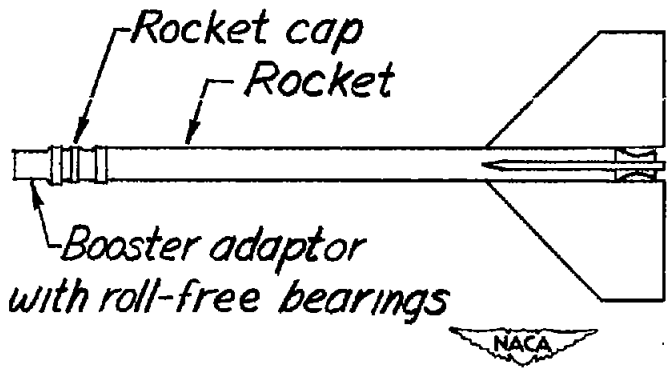

Booster Assembly

(a) Model and booster configurations.

Figure 1.– Dimensions of test missile model.

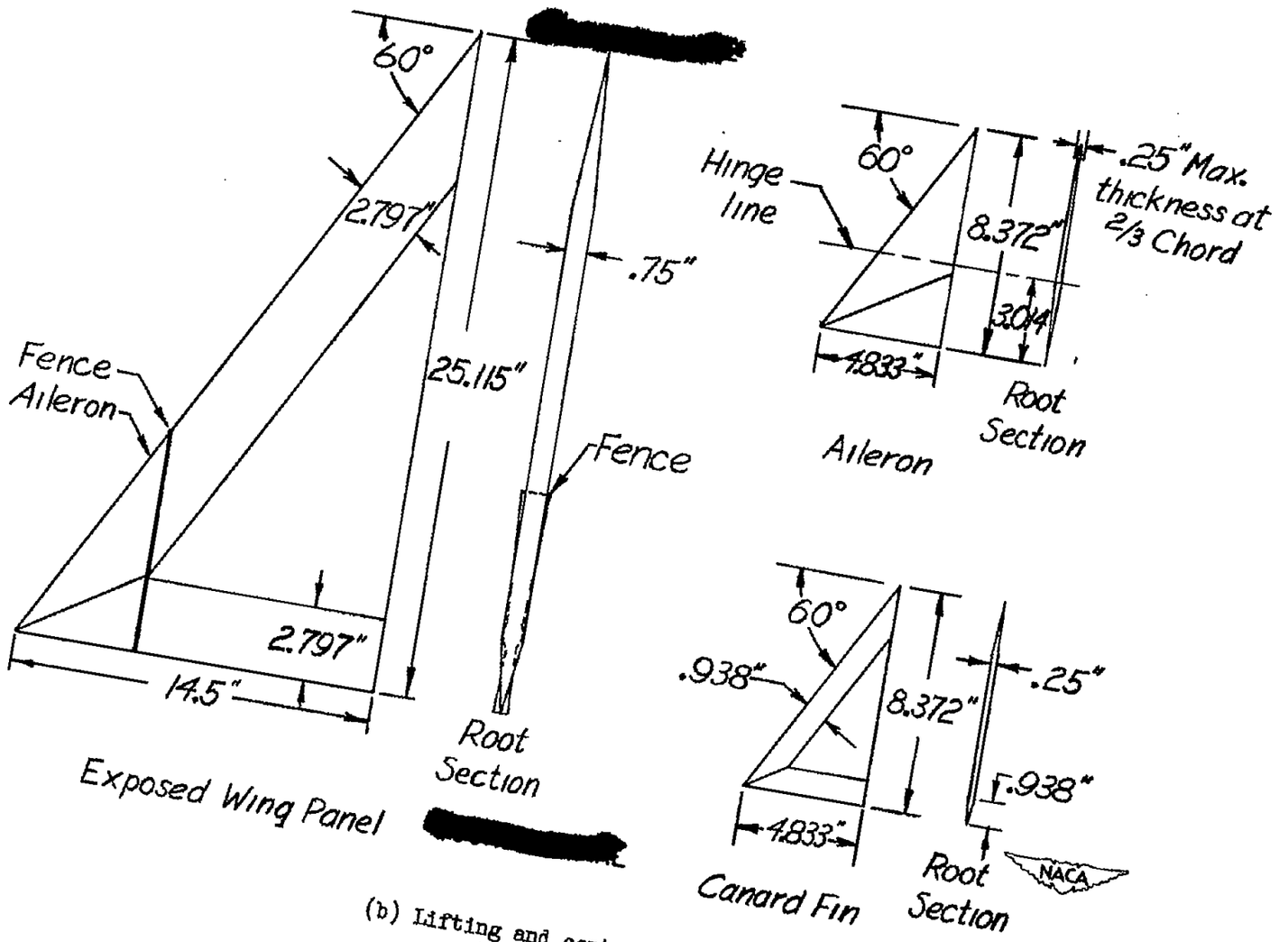

(b) Lifting and control surfaces.

Figure 1.– Concluded.

[redacted]

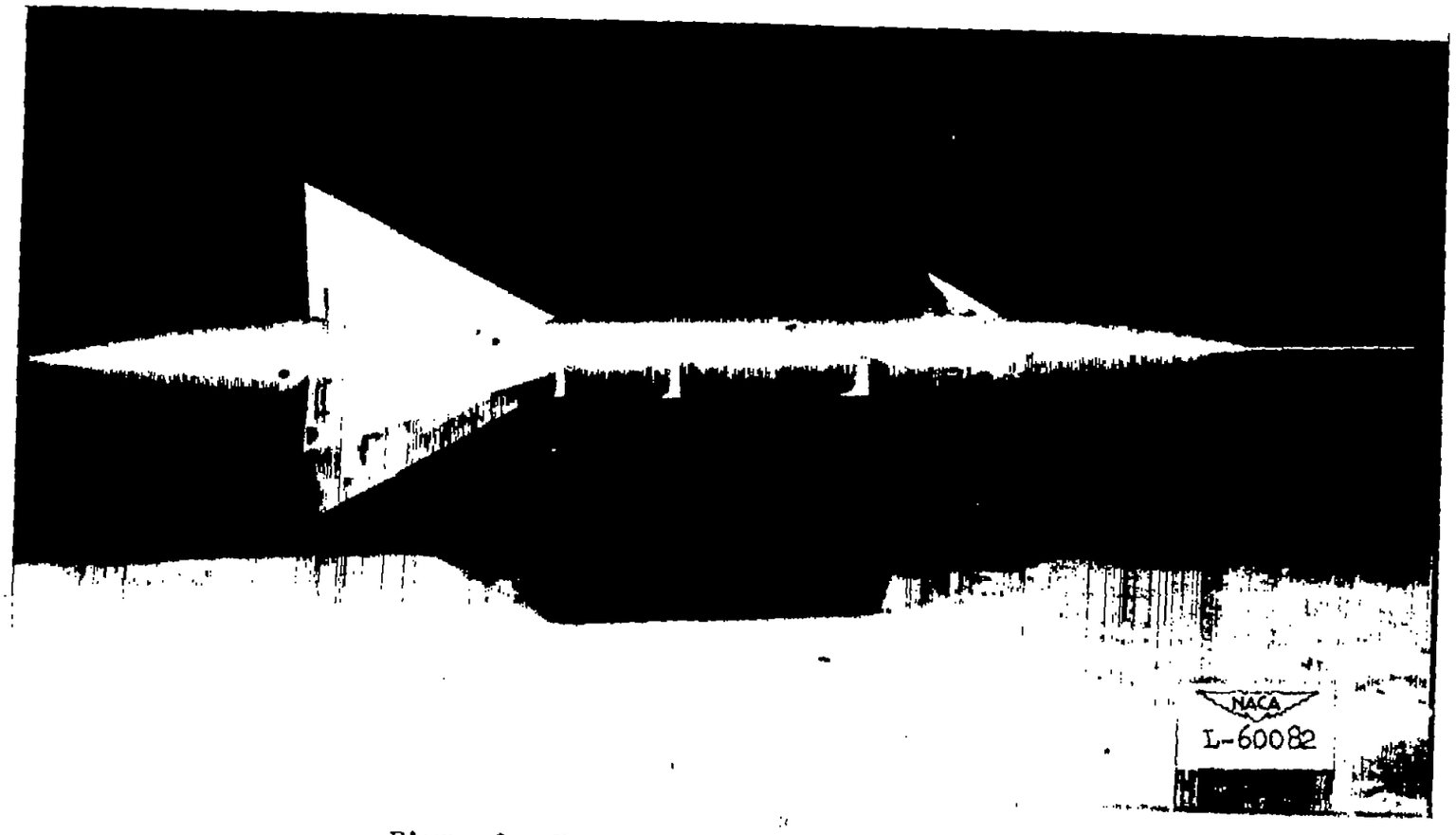

Figure 2.- Photograph of test missile model.

[redacted]

[redacted]

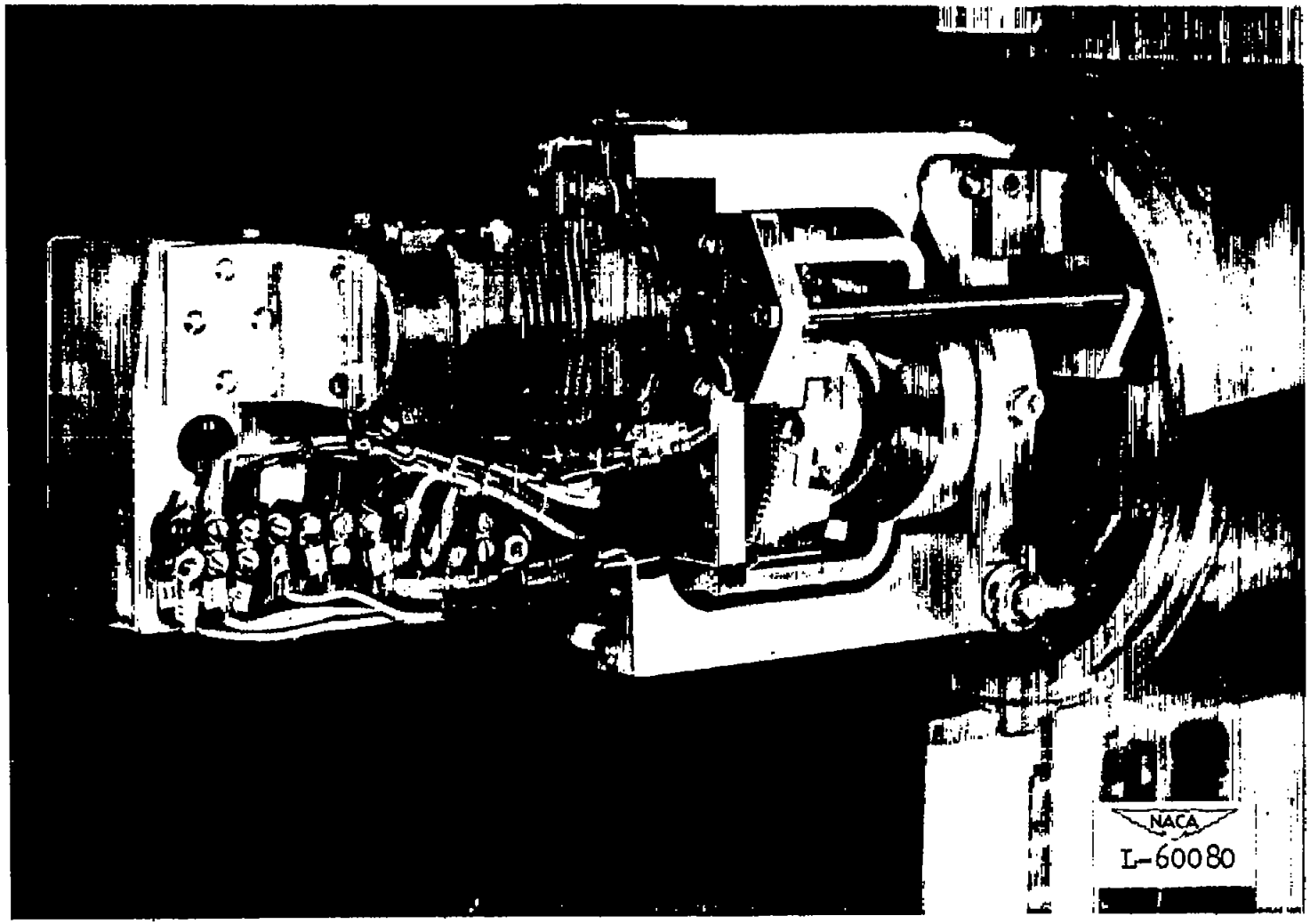

Figure 3.– Roll automatic pilot installed in missile model.

[redacted]

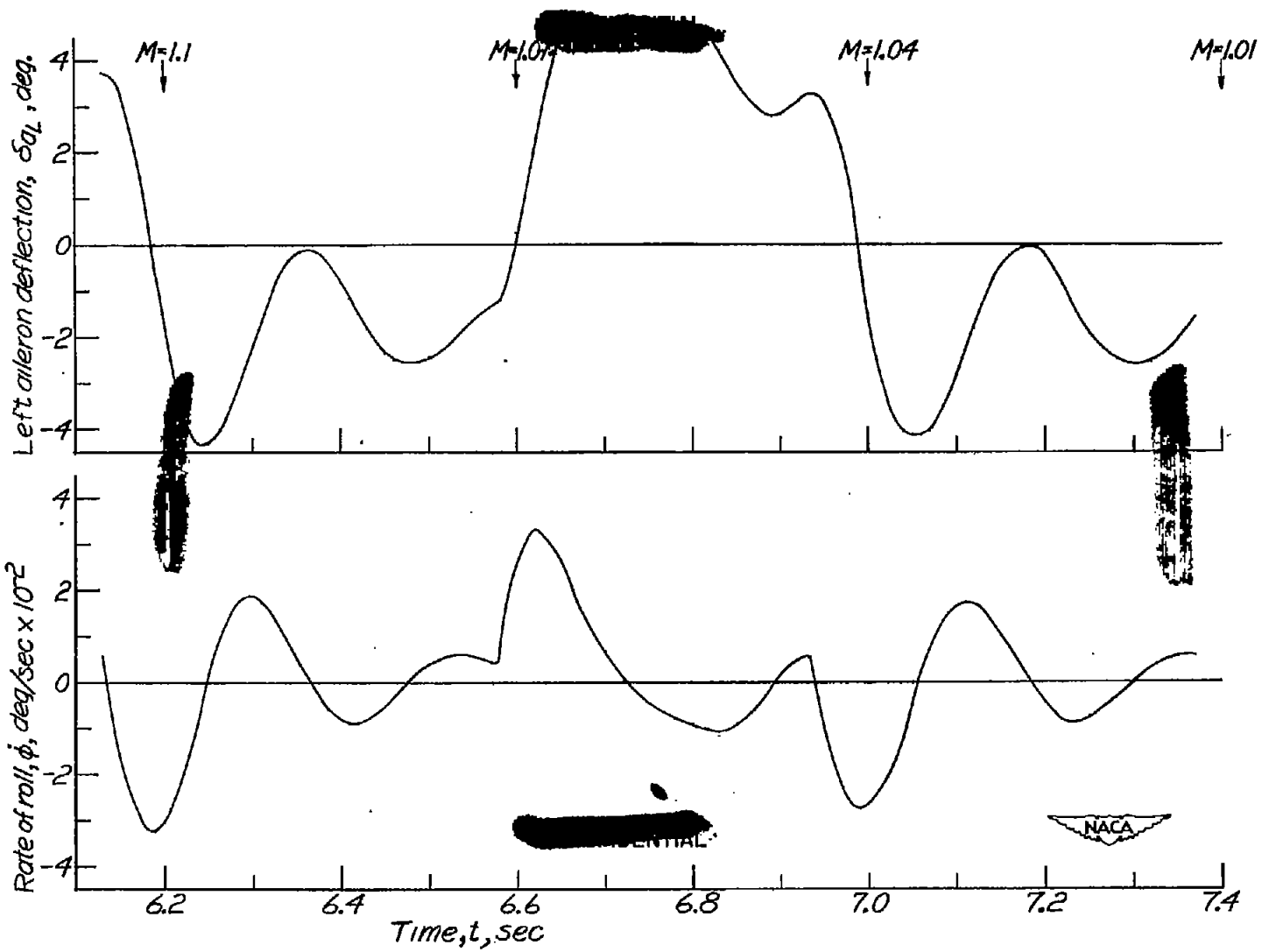

Figure 4.– Record of rate of roll and control-aileron position for $1\frac{1}{2}$-pulse aileron cycles in supersonic flight.

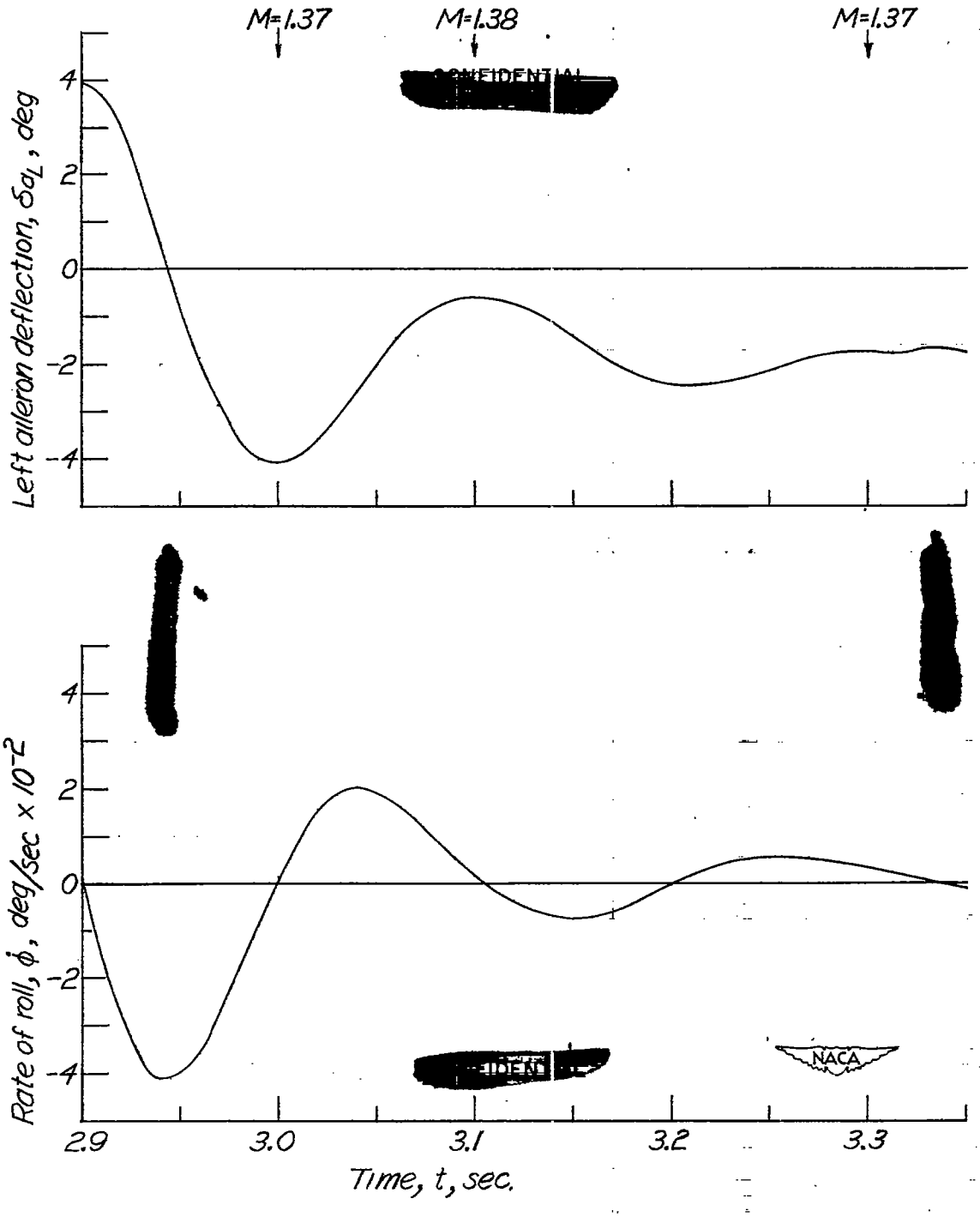

Figure 5.– Portion of rate of roll and control-aileron-position telemeter record at maximum flight Mach number and booster separation.

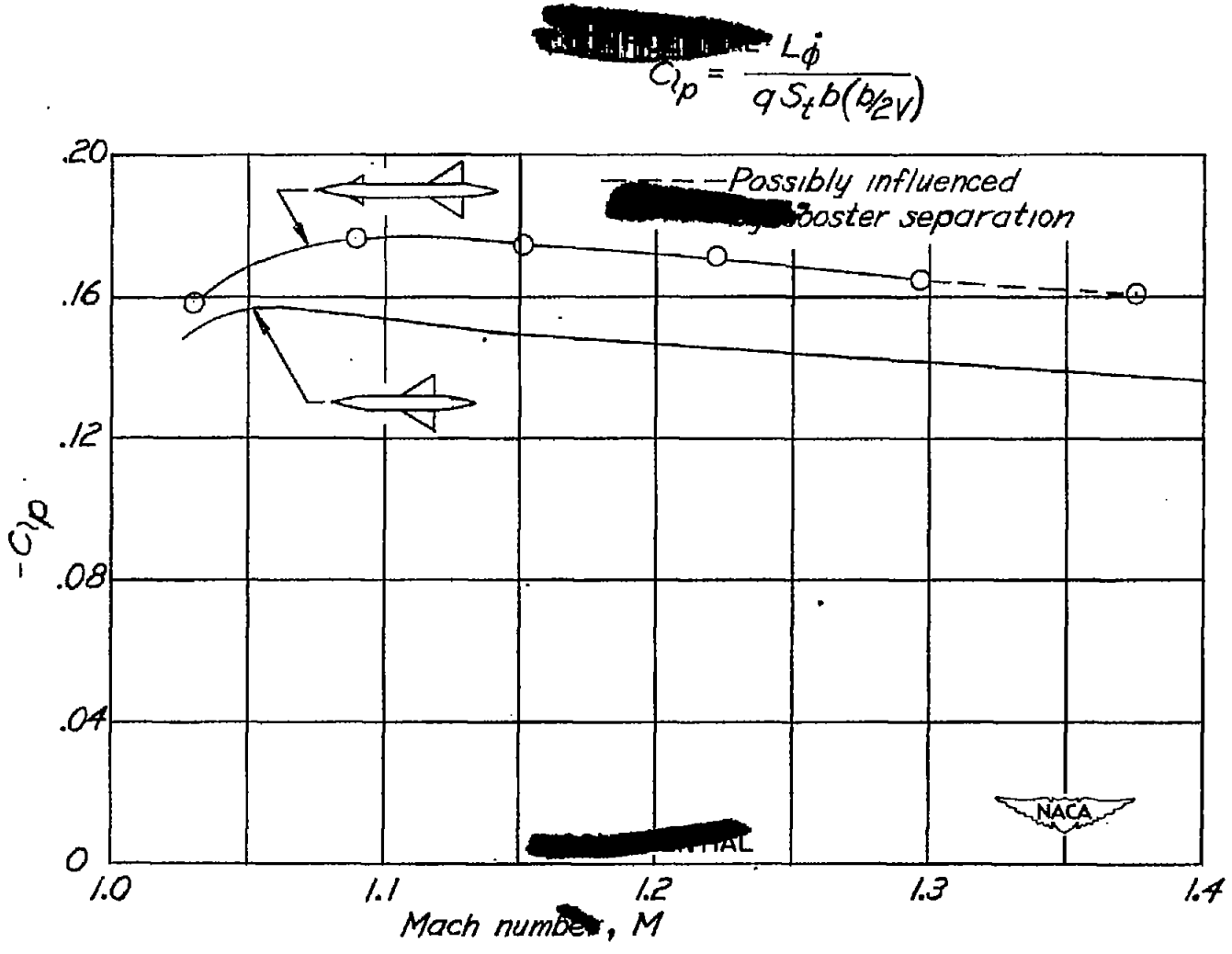

(a) Roll dam[redacted] C_{l_p}.

Figure 6.– Aerodynamic rolling derivatives determined from roll-velocity telemeter record and showing comparison with data of reference 2.

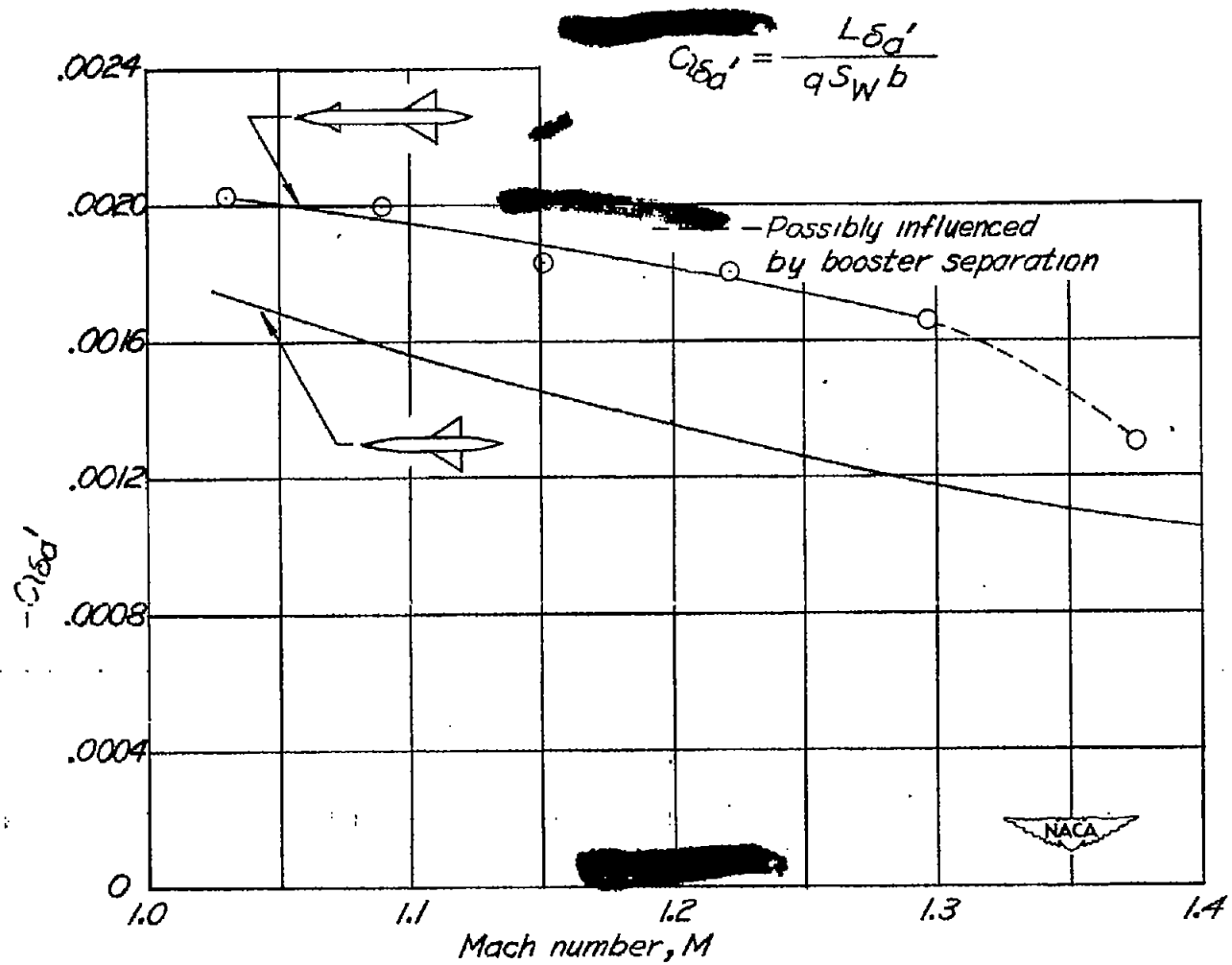

(b) Roll-con[redacted]ess derivative $C_{l_{\delta_a}}$.

Figure 6.– Concluded.

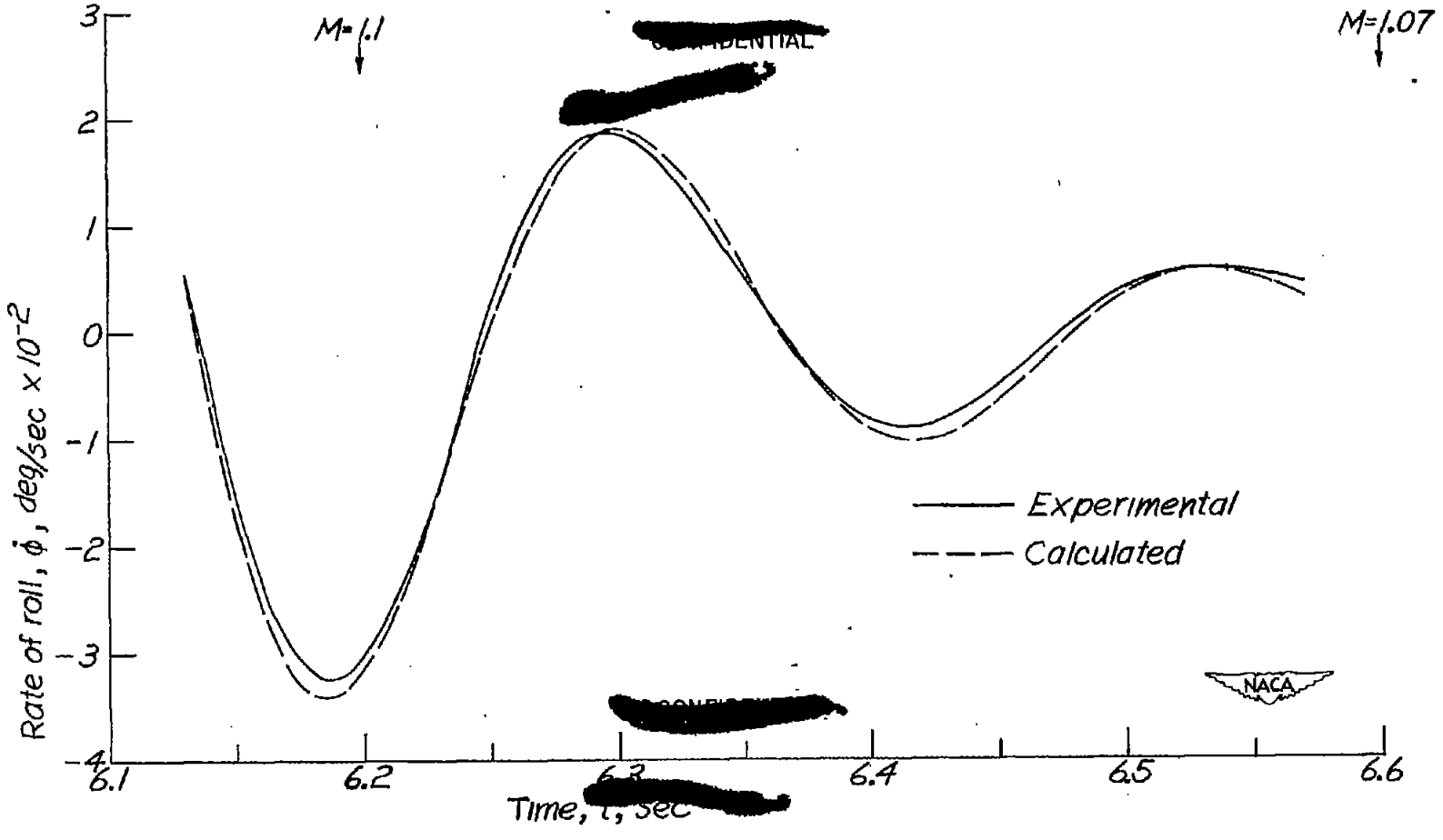

Figure 7.– Comparison of portion of rate-of-roll flight record and calculated rate-of-roll transient response to aileron pulse. Aerodynamic derivatives used in the calculation were those determined from the flight record.

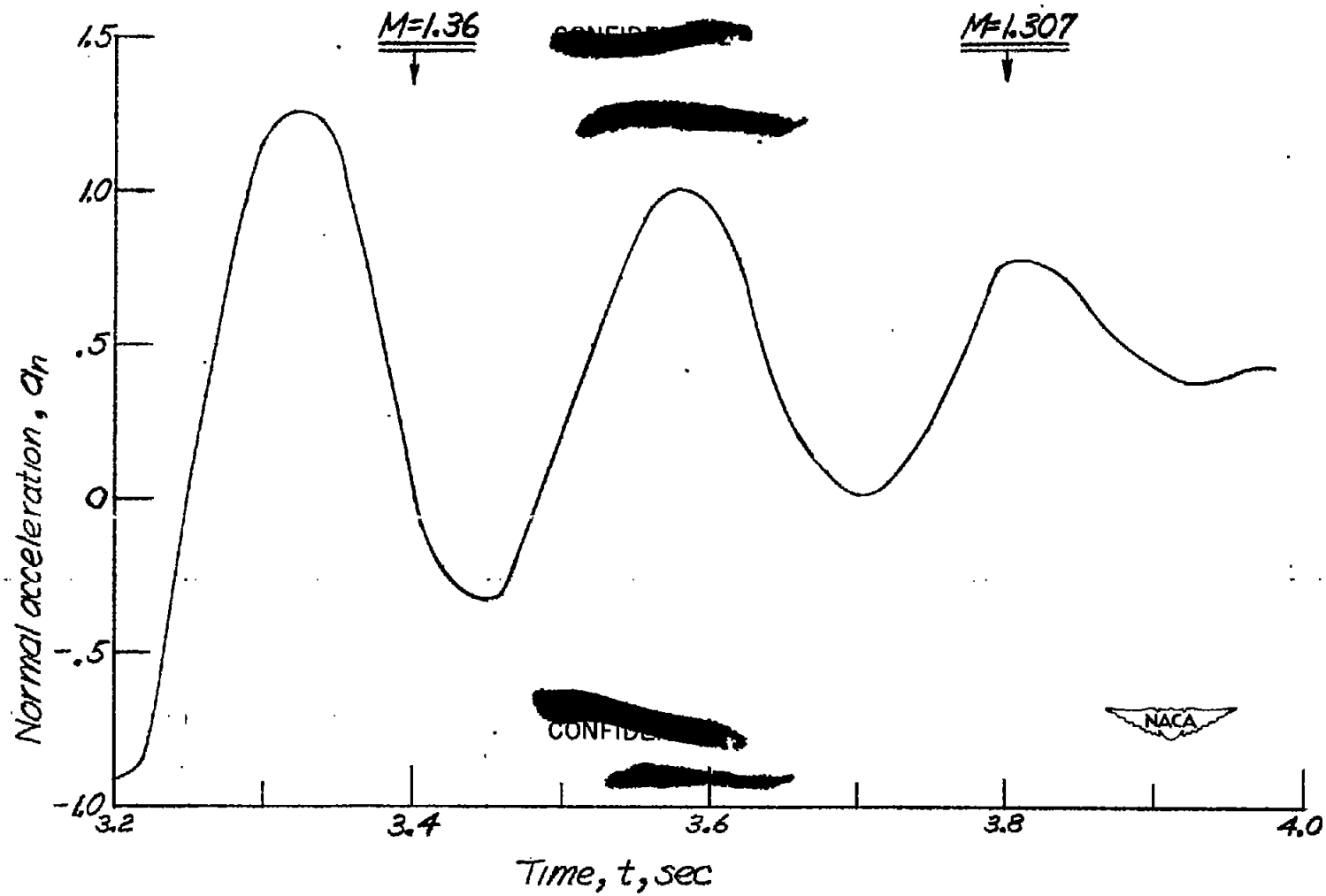

Figure 8.- Portion of normal-accelerometer-telemeter record showing transient oscillation.

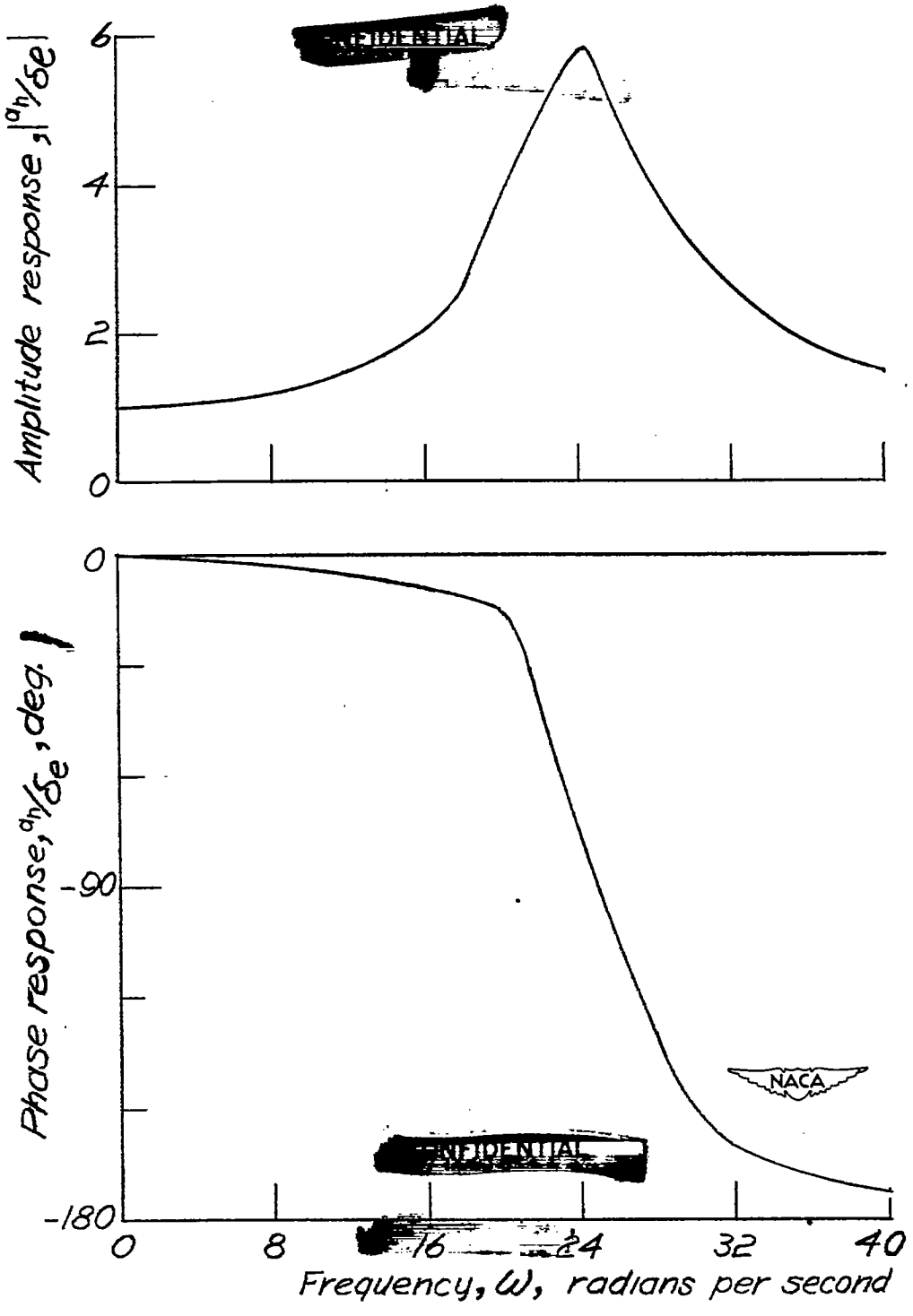

Figure 9.– Longitudinal frequency response as calculated from normal-acceleration transient response. Average Mach number, 1.33. (Amplitude shown is a_n/δ_e divided by the static (ω = 0) value of a_n/δ_e.)

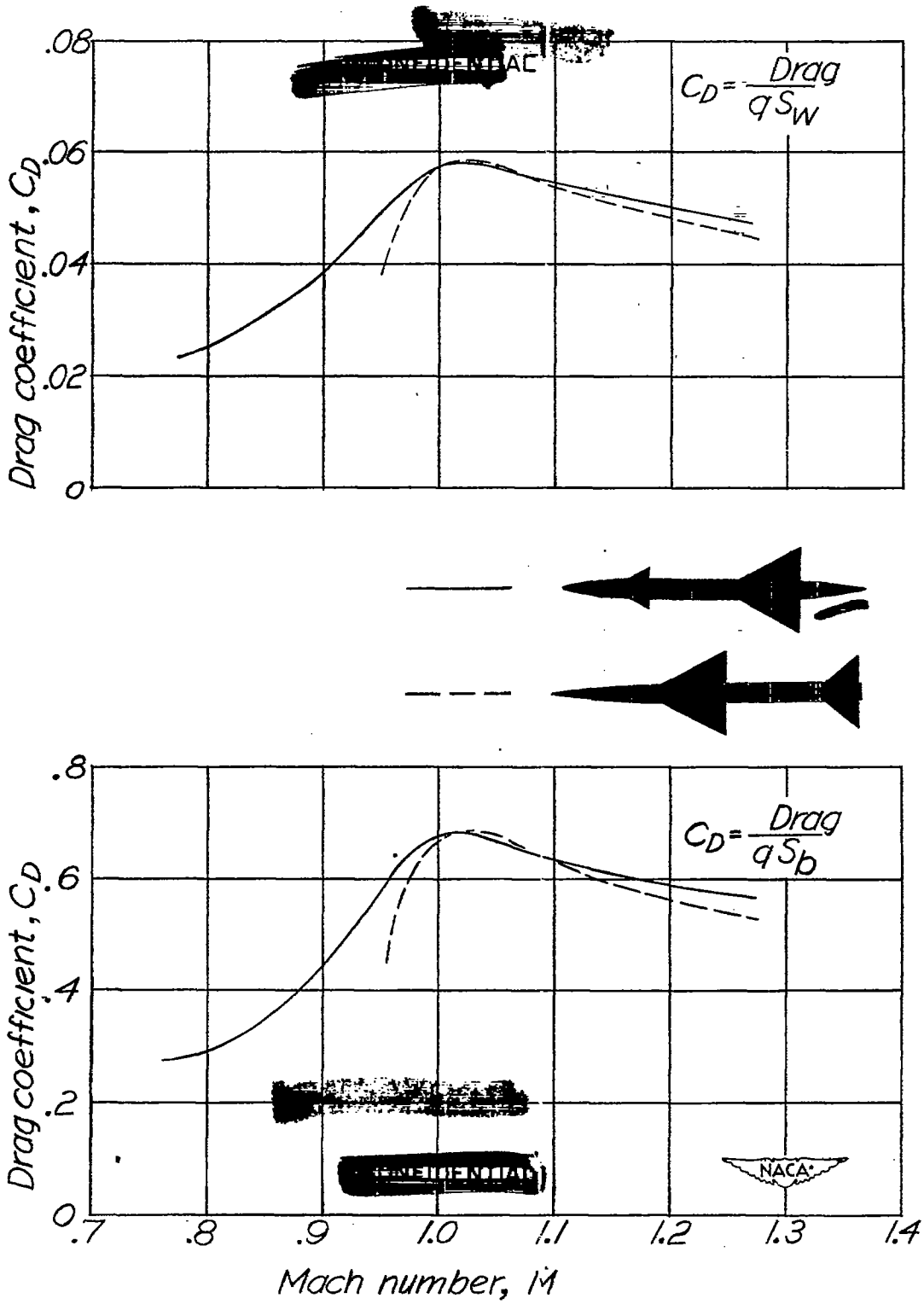

Figure 10.– Comparison of drag coefficients of the canard test-missile model and the comparable 4-percent-thick wing model.

[redacted]

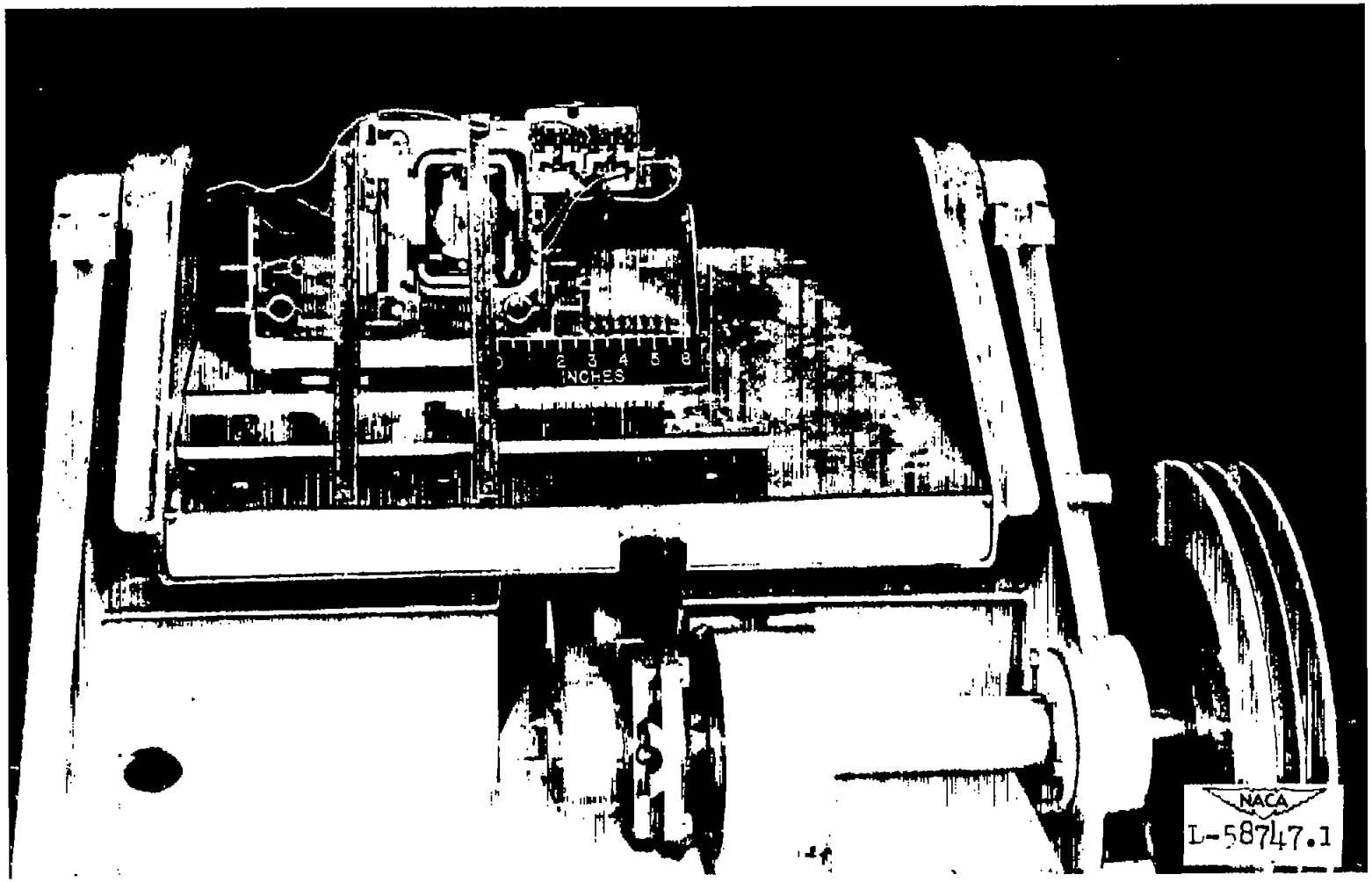

Figure 11.- Roll automatic pilot mounted on oscillating table for frequency-response tests.

[redacted]

[redacted]

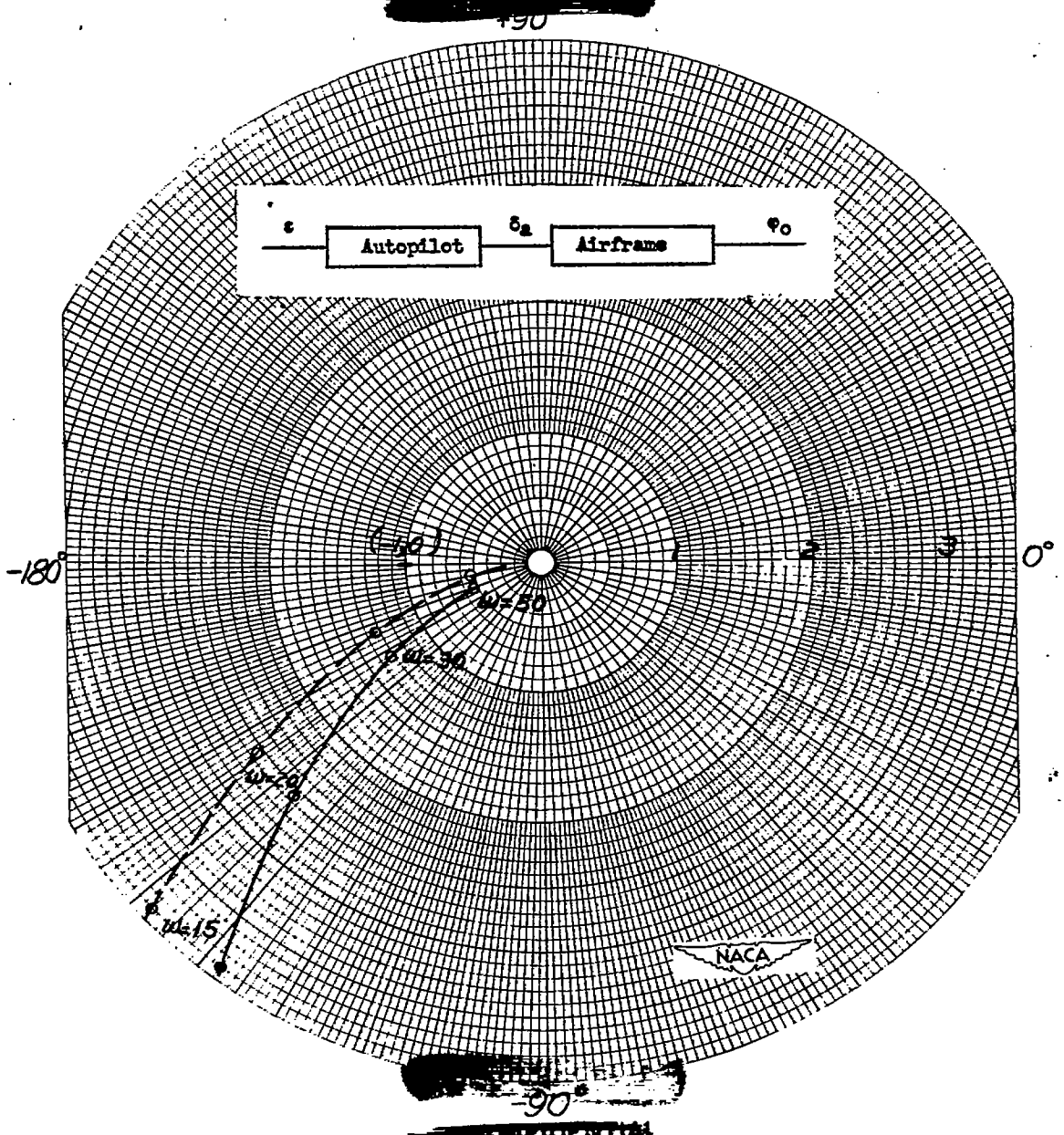

[redacted]

Figure 12.– Nyquist diagram of airframe and autopilot combination in roll utilizing calculated airframe frequency response and measured autopilot frequency response. K = 0.6. Broken curve indicates effect of 10° lag in the control system caused by large hinge moments.

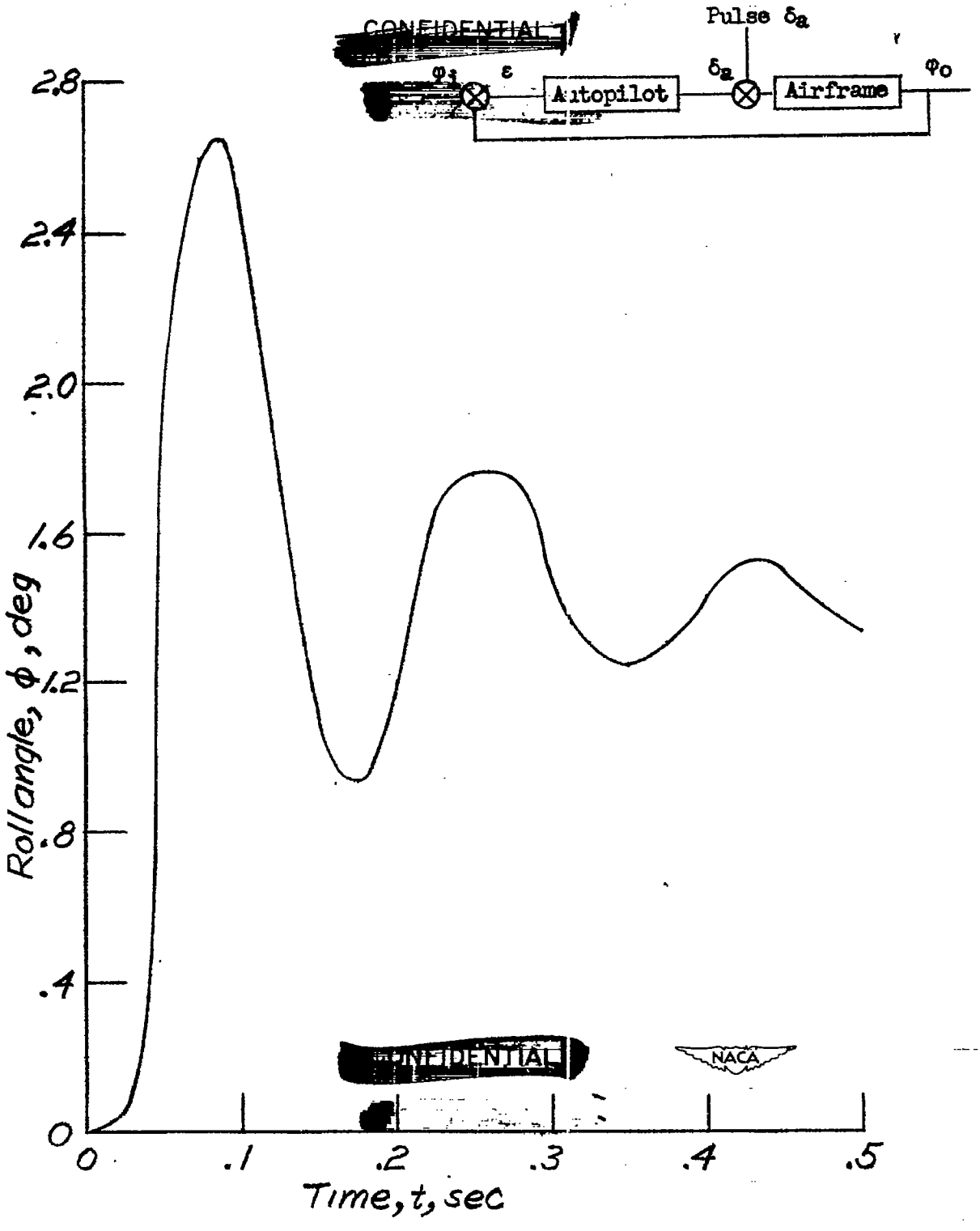

Figure 13.- Calculated airframe-and-autopilot-system transient response to a pulse aileron disturbance for preflight analysis.